ACTA IMEKO
ISSN: 2221-870X
December 2023, Volume 12, Number 4, 1 - 6

Realisation and characterisation of Cu-based references for neutron imaging calibration purposes and first results

Amina Vietti[1,4], Luisa Vigorelli[1,4], Sabrina Grassini[2,4], Laura Guidorzi[4], Marta Magalini[3,4], Alessandro Re[3,4], Alessandro Lo Giudice[3,4], Francesco Grazzi[5,6] , Nicla Gelli[5]

[1] *Politecnico di Torino, Dipartimento di Elettronica e Telecomunicazioni, Corso Duca degli Abruzzi 24, 10129 Torino, Italia*
[2] *Politecnico di Torino, Dipartimento di Scienza Applicata e Tecnologia, Corso Duca degli Abruzzi 24, 10129 Torino, Italia*
[3] *Università degli Studi di Torino, Dipartimento di Fisica, via Pietro Giuria 1, 10125 Torino, Italia*
[4] *Istituto Nazionale di Fisica Nucleare, sezione di Torino, via Pietro Giuria 1, 10125 Torino, Italia*
[5] *Istituto Nazionale di Fisica Nucleare, sezione di Firenze, via Sansone 1, 50019 Sesto Fiorentino (FI), Italia*
[6] *Consiglio Nazionale delle Ricerche, Istituto di Fisica Applicata "Nello Carrara", via Madonna del Piano 10, 50019 Sesto Fiorentino (FI), Italia*

ABSTRACT
The long-term purpose of this study is to assess the capabilities of the new Neutron Imaging beamline developed at the LENA facility of Pavia (Italy) for the characterisation of bronze artefacts. In this preliminary work, a set of Cu-based reference alloys has been produced and analysed in order to test and calibrate the facility. The first step involved the production of Cu-based alloys with chemical composition and microstructure similar to ancient artefacts. The chemical composition of the reference alloys was analysed by Optical Emission Spectroscopy. Secondly, some samples were artificially patinated with different chemical treatments obtaining an artificial corrosion products layer comparable to natural corrosion. X-Ray Diffraction, Scanning Electron Microscopy and Raman Spectroscopy have been used to characterise the corrosion patina. The main corrosion products on sulphate-induced patina are cuprite and brochantite, whereas atacamite and clinoatacamite were detected on chloride-induced patinas. Finally, preliminary Neutron Imaging measurements were performed on a first set of coated and uncoated specimens in order to try to correlate the neutrons attenuation coefficients with the chemical compositions with promising results.

Section: RESEARCH PAPER

Keywords: Neutron imaging; Cu-based artefacts; archaeological bronze; Raman spectroscopy; SEM-EDS

Citation: Amina Vietti, Luisa Vigorelli, Sabrina Grassini, Laura Guidorzi, Marta Magalini, Alessandro Re, Alessandro Lo Giudice, Francesco Grazzi, Nicla Gelli , Realisation and characterisation of Cu-based references for neutron imaging calibration purposes and first results, Acta IMEKO, vol. 12, no. 4, article 16, December 2023, identifier: IMEKO-ACTA-12 (2023)-04-16

Section Editor: Francesco Lamonaca, University of Calabria, Italy

Received October 23, 2023; **In final form** December 7, 2023; **Published** December 2023

Corresponding author: Amina Vietti, e-mail: amina.vietti@polito.it

1. INTRODUCTION

In the Cultural Heritage field, diagnostic techniques must satisfy a number of requirements such as the less invasiveness and not destructiveness of the analysis. In recent years, the number of non-invasive techniques has quickly grown up responding to this need. Concerning neutron-based techniques, Neutron Imaging represents an important tool for the study of Cultural Heritage artefacts thanks to the possibility to characterise both the surface and the bulk structure of the objects [1].

The mechanism behind absorption Neutron Imaging is basically represented by a neutron beam which passes through an object and produces an image on a detector that depends on the number of absorbed neutrons [2], [3]. This way it becomes clear that the functioning is very similar to classical X-ray Imaging, a technique widely used in the diagnostics of Cultural Heritage [4]. Most of the time, Neutron Imaging and X-ray Imaging provide complementary information about the material under investigation. It is possible to acquire both a 2D image (radiography) and a 3D image (tomography), in the latter case by using a rotating stage that allows the 180° rotation of the sample [5]. Neutron Imaging has many peculiarities that make it very suitable for the analysis of certain types of material: i) high penetration depth in rocks or metals, ii) high sensitivity to light elements, and iii) the possibility to discriminate between chemical elements close in the periodic table, seeing that the attenuation

coefficient of neutrons does not change linearly with the atomic number, Z [6]. Despite its great potential, the use of this technique is not so widespread due firstly to the limited availability of neutron sources and, secondly to the difficulty in obtaining measurements time in the large facilities with restricted access and, above all, high costs. Despite that, there is a growing interest in this technique, especially for the study and characterisation of metallic artefacts which represent an important category of archaeological finds.

In fact, metals have been widely used in the past, ever since man acquired the technology suitable for the extraction and the manufacturing of the matter. Archaeologists and scientists are interested in the study of ancient metals as it can provide different information about the manufacturing techniques [7], the use, the trades [8], the conservation state of an object [9] as well as on the corrosion products layers grown on the metallic surface due to the interaction with the environment [10]. In this scenario, Neutron Imaging represents an interesting analytical tool which can be coupled with conventional chemical and microstructural characterisation techniques for collecting information on the surface and the bulk features of metallic artifacts with the aim to answer archaeological and historical questions [11]-[13].

A new neutron facility has been developed in the framework of CHNet-NICHE project (NICHE: Neutron Imaging for Cultural HEritage) at the LENA Centre (Pavia, Italy). Before the analysis of real artefacts, it is therefore particularly important to calibrate the imaging beamline of the facility by using a set of reference specimens. In this way, it is possible to evaluate the mass attenuation coefficient as a function of the alloy composition and the thickness of the corrosion products layers.

2. MATERIALS AND METHODS

2.1. Reference alloys: production and characterisation

A large set of Cu-based reference alloys with metallurgical features and microstructure similar to ancient bronze artefacts were produced in laboratory [14], [15]. The selected chemical composition is ascribed to the material classes Cu-Sn, Cu-Zn and Cu-Sn-Pb. In particular, Cu-Sn and Cu-Zn alloys were produced by increasing the concentration of Sn and Zn in the range of 4-12 wt% and 5-25 wt%, respectively; the ternary alloy, Cu-Sn-Pb, was produced with a fixed amount of Sn (6 wt%) and by increasing the concentration of Pb in the range of 4-16 wt%.

The alloys were produced by using a Lindberg Blue STF54434C tube furnace. Alumina cylindrical crucibles (Al_2O_3 99% purity, base diameter of 2.5 cm, height of 7 cm) coated inside with graphite to avoid metal oxidation were used for metal melting. The alloys were melted under an inert atmosphere (Ar, 99% purity) in the tube furnace according to the following protocol: heating ramp from room temperature to 1250 °C in 2 hours, maintenance of temperature for 1 hour, cooling ramp from 1250 °C to room temperature in 5 hours. Then, the obtained ingots were cut in disks with a fixed thickness of 4 mm.

The Cu-based reference samples were then analysed by means of Optical Emission Spectroscopy (OES) by using a S7 Metal Lab Plus Quantometer to quantitatively determine the chemical composition after the melting.

Moreover, the metallographic analysis of the reference samples was performed to obtain information on the alloy's microstructure. The samples were embedded in acrylic resin, cut with a diamond saw and polished with diamond paste up to 1 μm; afterwards, the samples were chemically etched using a solution of $FeCl_3$ (1 g) - HCl (10 mL) - distilled water (100 mL) dipping the sample in the aggressive solution for 15 s according to the ASTM-E407-07 protocol [16]. The metallographic sections were observed using a Reichert-Jung MeF3 optical microscope at different magnifications.

Table 1. Chemical methods used for artificial corrosion on Cu-based specimens.

Solutions	Methods	Time
$CuSO_4$ 50 mM	Immersion	15 days
NH_4Cl 33 wt%	Immersion	7 days
NH_4Cl 33 wt%	Brushed	1 day
NH_4Cl 33 wt%	Dripped	1 day

2.2. Artificial patinas: synthesis and characterisation

A set of Cu-based reference alloys were previously polished with 500 to 4000-grid SiC paper, rinsed in ethanol in ultrasonic bath for 5 min, and dried. Then, two kinds of artificial patinas were grown on the metallic surface by means of a chemical synthesis in aqueous solutions containing copper sulphate ($CuSO_4$) and ammonium chloride (NH_4Cl) respectively, with the aim to obtain sulphate-patinas and chloride-patinas. The chemical solutions used to obtain the corrosion layers and the applying methods are briefly listed in Table 1.

Concerning the chemical patinas obtained by $CuSO_4$ the samples were immersed in a 50 mM solution for 15 days [17]; every 5 days, the samples were extracted from the solution, let them dry and photographed by using a XT-Fujifilm photo camera to evaluate the colour change and the patina growth.

Instead, chemical patinas obtained by NH_4Cl solutions [18] are represented by three different groups depending on the applications of solutions: immersion, dripped and brushed patinas. In the first case, the samples were immersed in a 33 wt% solution for 1 week letting them dry every 24 hours. In the second case, the 33 wt% solution was dripped on the surface letting it dry between one application and another for 1 day. In the last case, the samples were frequently brushed with the 33 wt% solution for 1 day, letting the surface dry between one brushing and another. At the end of the treatment, all the samples were photographed.

All the obtained patinas were characterised by means of Raman spectroscopy, X-Ray Diffraction (XRD) and Field Emission Scanning Electron Microscopy (FESEM).

The chemical composition of the artificial patinas was firstly analysed by a BWTEK i-Raman plus spectrometer equipped with a 532 nm excitation laser source, a CCD sensor with high quantum efficiency and wide dynamic range assisted by a cooling system and connected with an OPTEKA microscope equipped with different optics (4×, 20×, 40×, and 80×). All spectra were collected in the range from 150 cm^{-1} to 4200 cm^{-1} with a resolution of 5 cm^{-1}. The laser power was modulated to avoid chemical degradation of the sample due to laser radiation according to literature [19]. The acquisition parameters were set before measurement: 5 s integration time, 5 repetitions and laser power of 20%. The spectra processing was performed by using the BWSpec software and the identification was possible by comparing the obtained spectra with the RRUFF database [20] and literature [21], [22].

Additionally, chemical and microstructural characterisations were performed by using a Panalytical X'pert PRO diffractometer equipped with a Cu-anode. XRD analysis were performed by setting the tube current and the tube tension at

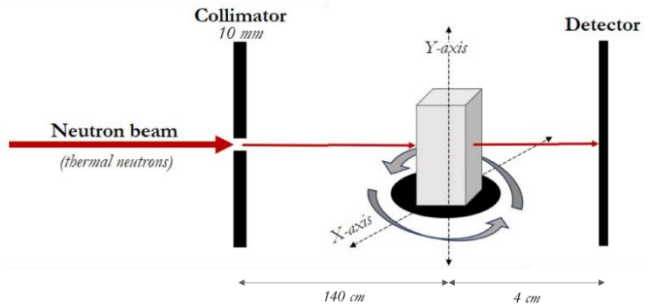

Figure 1. Experimental setup of the imaging beamline at the LENA facility (Pavia, Italy).

40 mA and 40 kV, respectively. Diffractograms were acquired in the range of 8°2θ to 90°2θ with a measure step of 0,026°2θ. The identification of the corrosion products was made by using the HighScore plus software.

The surface morphology was observed by means of a Zeiss Supra 40 FESEM microscope with secondary electron detector. The FESEM images were acquired using an acceleration voltage of 5 kV and an aperture size of 30 μm. The magnification was modulated depending on the dimension of the crystals.

2.3. Neutron Imaging and image processing

Neutron Imaging analyses were performed at the imaging beamline at the LENA facility. The facility consists of a TRIGA MARK II reactor which has a nominal power (in steady state) of 250 kW and a maximum neutron flux of 1.8 × 1013 cm^{-2} s^{-1} [23]. Neutrons are slowed down to thermal energies (25 meV) in order to be suitable for Neutron Imaging analyses. In Figure 1, a schematic representation of the setup is shown. The following parameters were used for the acquisition of images: distance from the collimator to the object 140 cm, distance from the object to the detector 4 cm, and the pinhole aperture 10 mm. The detector consists of an Ag-doped 300 μm thickness ^{6}LiF/ZnS scintillator, a mirror, and a CCD camera. The acquisition time for each image was 300 s. The object is positioned on a sample-holder that can move on X and Y directions, thus allowing to leave the detector stationary. In case of tomography, the sample-holder can rotate around 180° All movements are remotely controlled by software.

The image processing was carried out using the ImageJ open-source software, applying some correction to calculate the grey levels within the image. The first fundamental correction consists in subtracting the dark (the acquisition with the beam turned off) from the raw image of the sample and then dividing this result by the image obtained by subtracting the dark from the white (the acquisition with the beam turned on without any samples). From the final image, a 50 × 50 $pixel^2$ region of interest was considered to obtain the average grey level value for each sample.

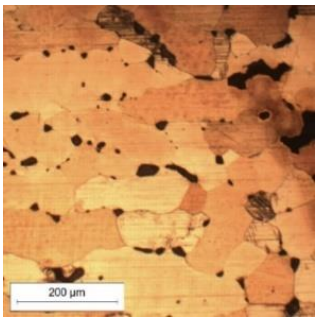

Figure 2. Microstructure of the CuSn6Pb4 reference alloy.

Table 2. Chemical composition of the Cu-based reference samples obtained by Optical Emission Spectroscopy

Sample	Cu(wt%)	Sn(wt%)	Pb(wt%)	Zn(wt%)
CuZn5	94.7 ± 0.8	-	-	5.1 ± 0.8
CuZn10	90.9 ± 0.9	-	-	9.0 ± 0.9
CuZn15	85.6 ± 0.9	-	-	14.3 ± 0.9
CuZn20	81.5 ± 1.1	-	-	18.4 ± 1.1
CuZn25	78.6 ± 1.5	-	-	21.3 ± 1.5
CuSn4	95.2 ± 0.4	4.7 ± 0.4	-	-
CuSn6	93.5 ± 0.5	6.5 ± 0.5	-	-
CuSn9	90.2 ± 0.4	9.8 ± 0.4	-	-
CuSn12	88.8 ± 0.5	11.1 ± 0.5	-	-
CuSn6Pb4	89.0 ± 0.6	6.1 ± 0.2	4.8 ± 0.5	-
CuSn6Pb8	84.2 ± 1.2	5.9 ± 0.3	9.8 ± 0.9	-
CuSn6Pb12	79.6 ± 1.1	6.3 ± 0.1	14.0 ± 1.1	-
CuSn6Pb16	73.9 ± 1.6	5.0 ± 0.4	21.0 ± 1.4	-

Then, the Lambert-Beer equation was used to calculate the different attenuation coefficients.

3. RESULTS AND DISCUSSION

3.1. Reference alloys characterisation

The OES results basically confirmed the expected percentage of elements after the furnace melting, except for the set that includes the CuSnPb samples; in fact, a higher percentage of Pb and a nonhomogeneous distribution of Pb in the alloy was observed. The results obtained are shown in Table 2. A plausible explanation is that Cu and Pb have very different melting temperatures (Cu 1085 ˚C and Pb 327.5 °C) forcing the diffusion and the segregation of Pb in different areas of the sample at the expense of Cu. Further detailed analyses are needed to characterise properly the different grains, to evaluate the presence of solid solutions and different phases.

The microstructure of the alloy can be evidenced thanks to the chemical etching. An example of the microstructure of CuSn6Pb4 alloy is given in Figure 2. Poly-crystalline grains with variable size (from 50 μm to 400 μm depending on the orientation) with some dendrites. Pb is present as pure lead globules in the grain boundaries.

3.2. Sulphates-induced patinas characterisation

Sulphates-induced patinas (Figure 3) are characterised by a layer of about 20 μm of thickness, with a dark green colour. The main corrosion products found on the surface are brochantite ($Cu_4SO_4(OH)_6$) and cuprite (Cu_2O), confirmed by Raman Spectroscopy and X-Ray Diffraction. Macroscopically, the layer is apparently compact and uniform. Thanks to the high-resolution FESEM images it is possible to underline a good, layered morphology, with well crystallized corrosion products.

3.3. Chlorides-induced patinas characterisation

The corrosion products found on chlorides-induced patinas (Figure 4) are mainly atacamite and clinoatacamite ($Cu_2Cl(OH)_3$), confirmed by Raman spectroscopy and XRD analyses. The average thickness of the corrosion products layer is about 150 μm, and the colour is mainly light blue. The patina is quite compact but not uniformly distributed on the metal surface, as it is possible to observe also macroscopically. The corrosion products layer is full of cracks and tends to peel off. The high-resolution FESEM images underline the fragility of the corrosion patina.

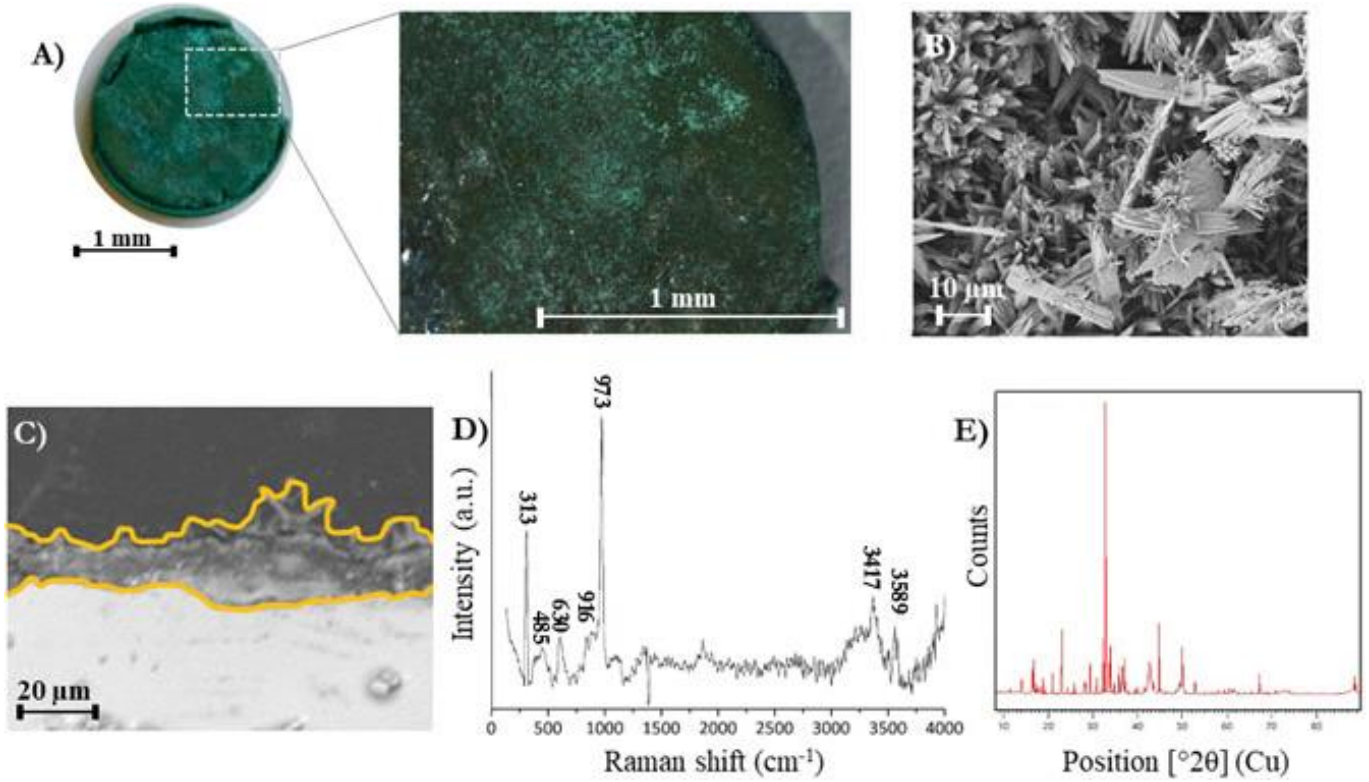

Figure 3. Obtained results on CuSn6Pb4 alloy sample immersed in $CuSO_4$ solution 50 mM for 15 days. In particular, A) high-quality image of the sample and superficial enlargement, B) FESEM image of the surface morphology, C) FESEM image of sample section, D) Raman spectrum and E) XRD diffractogram.

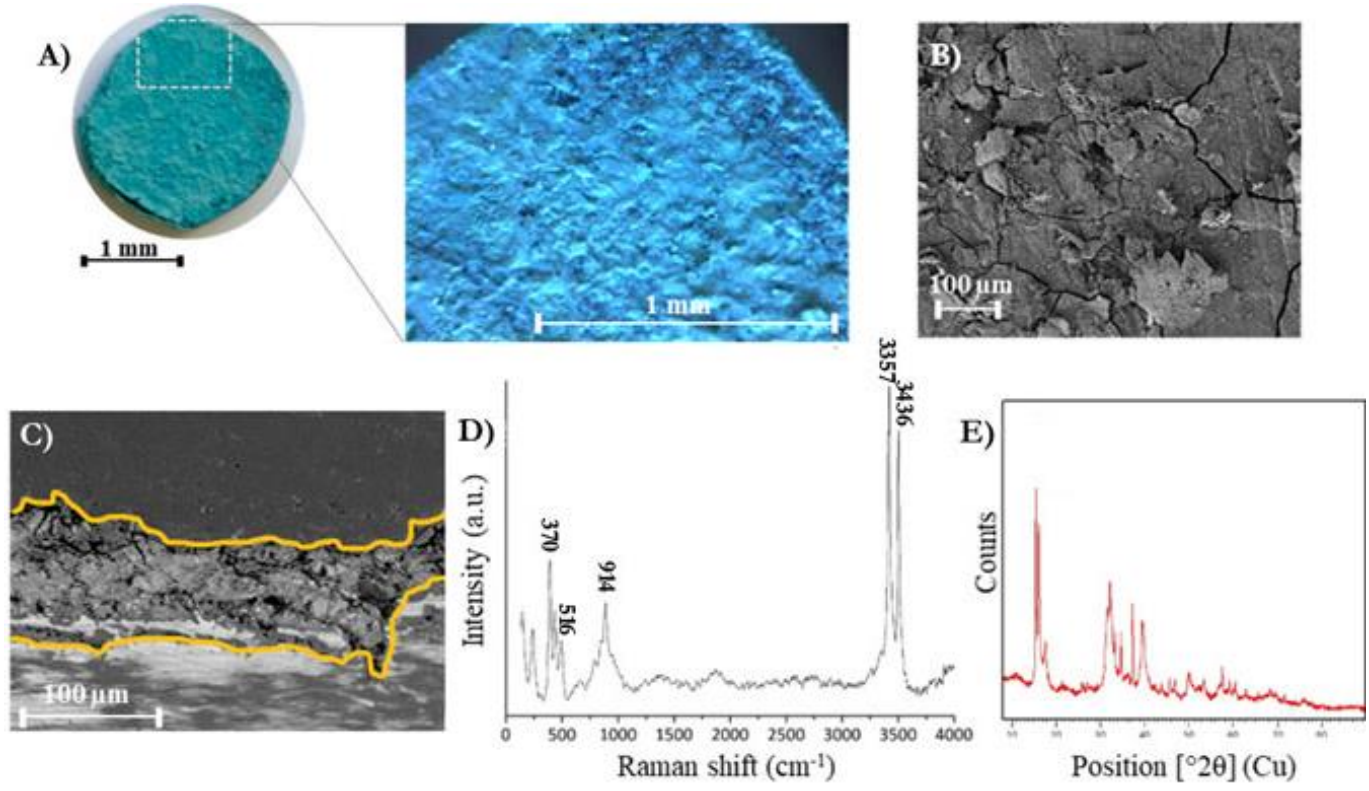

Figure 4. Obtained results on CuSn4 alloy sample brushed with NH_4Cl solution 33 wt% for 1 day. In particular, A) high-quality image of the sample and superficial enlargement, B) FESEM image of the surface morphology, C) FESEM image of sample section, D) Raman spectrum and E) XRD diffractogram.

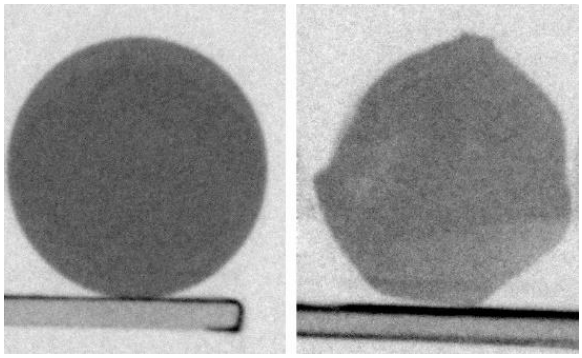

Figure 5. Example of Neutron radiography of pure Cu (left) and CuZn20 (right) reference.

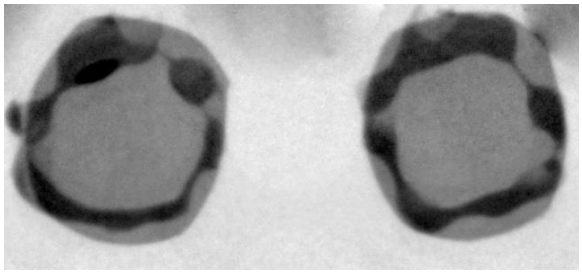

Figure 6. Example of Neutron radiography of CuSn6Pb4 specimens with sulphate-induced patina (left) and chloride-induced patina (right). The dark halos are due to the glue used to fix the samples to the support.

3.4. Neutron Imaging: preliminary data

A set of Cu-based alloys specimens was analysed by means of Neutron Imaging. The analyses were carried out on samples with different percentages of copper and, in a preliminary manner, on some patinated samples. The principal aim was the evaluation of the attenuation mass coefficient of the samples in function of the chemical composition. All the attenuation mass coefficients were calculated from a 50x50 pixel region of interest obtaining the average grey level value for each sample.

As an example, the CuZn specimens presents a variation in the attenuation coefficient compared to pure Cu. Since the attenuation coefficient of the sample is dominated by the contribution of Cu over the Zn, a decrease of the coefficient value is expected when the Zn content in the alloy increases. Only pure Cu and CuZn20 (Figure 5) were taken into consideration to present these preliminary results about the attenuation mass coefficient. However, more work is needed in the future with the aim of reducing the error associated with the obtained results to be able to draw more realistic conclusions. Further measurements on more specimens to better discriminate the differences, even minimal, in the chemical composition. Unfortunately, at the moment is possible only to discriminate samples with a large compositional difference.

Only few corroded samples were analysed (Figure 6), in particular a set of chlorides-induced and sulphates-induced patinas. Some results obtained on coated samples (CuSn6Pb4 sample) are represented in Figure 7. From the obtained radiography is not possible to make considerations on the different compositions between the patina and the bulk. Only tomography could provide this kind of information, as the flat geometry of the sample and the perpendicularity of the beam do not allow the different contributions to be distinguished. In this regard, tomographic analyses will be carried out on these samples in the near future.

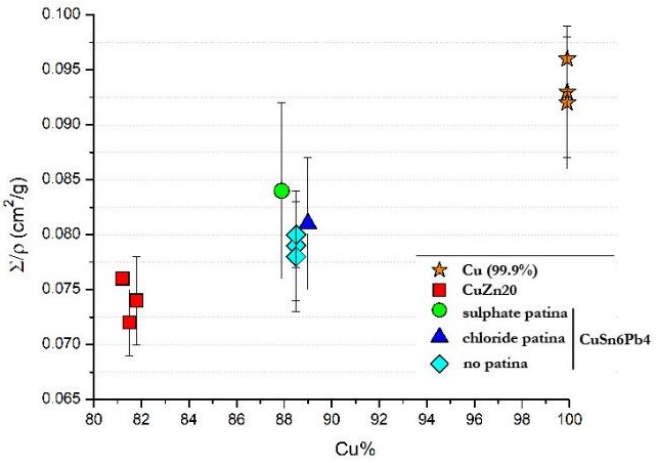

Figure 7. Evaluation of attenuation mass coefficient according to different composition (pure Cu and CuZn alloy with Zn 20 wt%); some preliminary results obtained on coated samples (CuSn6Pb4) are also represented in function of the attenuation mass coefficient.

4. CONCLUSIONS

In the present paper, several Cu-based alloy specimens have been prepared in laboratory to obtain references for Neutron Imaging calibration purposes. The first important point was the full characterisation of the chemical composition of the produced alloys, obtaining the percentage of elements (Cu, Sn, Pb and/or Zn) after the melting. Afterwards, different chemical treatments have been tested on Cu-based samples in order to obtain various patinas characterised by well-defined chemical composition and morphology.

The use of Neutron Imaging in the characterisation of uncoated specimens (binary CuSn and CuZn, and tertiary CuSnPb) looks very promising, whereas on the contrary, the corroded samples require deeper investigation. Concerning chloride-induced patina, further chemical preparation will be carried out avoiding problems encountered in this analysis (i.e., not uniform distribution on the metal surface, fragility of the coating, and presence of cracks).

About Neutron Imaging, differences were observed in the absorption coefficient between Cu and CuZn alloy, but not between samples with patina. To this end, it will be fundamental to perform 3D tomography in order to evaluate firstly the influence of the corroded surface on the obtained image and, secondly, the thickness and the composition of both patina and bulk. To carry out tomography the minimum required thickness of 150 μm will be taken in account. This is a crucial point for the coated samples obtained with the aqueous solution containing copper sulphate which presents a very thin layer of corrosion products.

ACKNOWLEDGEMENTS

This project has been funded by Istituto Nazionale di Fisica Nucleare (INFN, Italy), CHNet-NICHE CSN 5 experiment. The authors would like to thank all the people involved in the project and the LENA personnel.

REFERENCES

[1] E. Lehmann, D. Mannes, A. Kaestner, C. Grünzweig, Recent Applications of Neutron Imaging Methods, Physics Procedia, vol. 88 (2017), pp. 5-12.
DOI: 10.1016/j.phpro. 2017.06.055

[2] N. Kardjilov, G. Festa, Neutron methods for archaeology and cultural heritage. Springer, 2017, ISBN 978-3319331614

[3] W. Kockelmann, L.C. Chapon, R. Engels, J. Schelten, C. Neelmeijer, H.M. Walcha, G. Artioli, S. Shalev, E. Perelli-Cippo, M. Tardocchi, G. Gorini, P.G. Radaelli, Neutrons in cultural heritage research. Journal of Neutron Research, vol. 14 (2006) 1, pp. 37-42.
DOI: 10.1080/10238160600673284

[4] L. Vigorelli, A. Re, P. Buscaglia, N. Manfredda, M. Nervo, T. Cavaleri, P. Del Vesco, M. Borla, S. Grassini, L. Guidorzi, A. Lo Giudice, Comparison of two ancient Egyptian Middle Kingdom statuettes from the Museo Egizio of Torino through computed tomographic measurements, Journal of Archaeological Science: Reports, vol. 44 (2022), art. no. 103518.
DOI: 10.1016/j.jasrep.2022.103518

[5] E. H. Lehmann, E. Deschler-Erb, A. Ford, Neutron tomography as a valuable tool for the non-destructive analysis of historical bronze sculptures, Archaeometry, vol. 52 (2010) 2, pp. 272-285.
DOI: 10.1111/j.1475-4754.2009.00480.x

[6] I. S. Anderson, R. L. McGreevy, H. Z. Bilheux, Neutron imaging and applications. No. 2209, Springer, 2009.

[7] T. De Caro, The ancient metallurgy in Sardinia (Italy) through a study of pyrometallurgical materials found in the archaeological sites of Tharros and Montevecchio (West Coast of Sardinia). Journal of Cultural Heritage, vol. 28 (2017) pp. 65-74.
DOI: 10.1016/j.culher.2017.05.016

[8] D. Dungworth, Roman copper alloys: analysis of artefacts from northern Britain, Journal of Archaeological Science, vol. 24 (1997) 10, pp. 901-910.
DOI: 10.1006/jasc.1996.0169

[9] D. Watkinson, Degree of mineralization: its significance for the stability and treatment of excavated ironwork, Studies in Conservation, vol. 28 (1983) 2, pp. 85-90.
DOI: 10.2307/1506054

[10] A. Vietti, E. Angelini, S. Grassini, N. Donato, Raman spectroscopic characterization of corrosion products of archaeological iron, Proc. of the 2021 Int. Conf. on Metrology for Archaeology and Cultural Heritage (MetroArchaeo 2021) Milan, Italy, 20-22 October 2021, Journal of Physics: Conference Series, vol. 2204, No. 1, 2021, p. 012066.
DOI 10.1088/1742-6596/2204/1/012066

[11] E. H. Lehmann, D. Mannes, M. Henss, M. Speidel, Ancient Buddhist metal statues using neutron tomography. In Handbook of Cultural Heritage Analysis, (2022) pp. 273-303. Cham: Springer International Publishing.
DOI: 10.1007/978-3-030-60016-7_11

[12] F. Salvemini, A. Williams, D. Edge, B. Schillinger, F. Cantini, F. Grazzi, On the use of neutron imaging methods to identify microstructural features in ancient Indian swords and armour, Microchemical journal, vol. 159 (2020), art. no. 105397.
DOI: 10.1016/j.microc.2020.105397

[13] A. Fedrigo, M. Strobl, A. R. Williams, K. Lefmann, P. E. Lindelof, L. Jørgensen, P. Pentz, D. Bausenwein, B. Schillinger, A. Kovyakh, F. Grazzi., Neutron imaging study of 'pattern-welded' swords from the viking age, Archaeological and Anthropological Sciences, vol. 10 (2018) 6, pp. 1249-1263.
DOI: 10.1007/s12520-016-0454-5

[14] D. A. Scott, Metallography and microstructure in ancient and historic metals. Getty publications, 1992. ISBN 0892361956

[15] P. T. Craddock, The composition of the copper alloys used by the Greek, Etruscan and Roman civilizations: 3. The origins and early use of brass, Journal of Archaeological Science, vol. 5 (1978) 1, pp. 1-16.
DOI: 10.1016/0305-4403(78)90015-8

[16] "ASTM-E407-07 - Standard practice for microetching metals and alloys," ASTM International: West Conshohocken, PA, USA, 2015.

[17] G. Di Carlo, C. Giuliani, C. Riccucci, M. Pascucci, E. Messina, G. Fierro, M. Lavorgna, G. Ingo, Artificial patina formation onto copper-based alloys: Chloride and sulphate induced corrosion processes, Applied Surface Science, vol. 421 (2017), pp. 120-127.
DOI: 10.1016/j.apsusc.2017.01.080

[18] K. Marušić, H. Otmačić-Ćurković, Š. Horvat-Kurbegović, H. Takenouti, E. Stupnišek-Lisac, Comparative studies of chemical and electrochemical preparation of artificial bronze patinas and their protection by corrosion inhibitor, Electrochimica Acta, vol. 54 (2009) 27, pp. 7106-7113.
DOI: 10.1016/j.electacta.2009.07.014

[19] L. Es Sebar, L. Iannucci, Y. Goren, P. Fabian, E. Angelini, S. Grassini, Raman investigation of corrosion products on Roman copper-based artefacts, Acta IMEKO, vol. 10 (2020) 1, pp. 129-135.
DOI: 10.21014/acta_imeko.v10i1.858

[20] B. La Fuente, R.T. Downs, H. Yang, N. Stone, The power of databases: the rruff project, in Highlights in mineralogical crystallography, 2015, De Guyter, pp. 1-30.

[21] F. Ospitali, C. Chiavari, C. Martini, E. Bernardi, F. Passarini, L. Robbiola, The characterization of Sn-based corrosion products in ancient bronzes: a Raman approach, Journal of Raman Spectroscopy, vol. 43 (2012) 11, pp. 1596-1603.
DOI: 10.1002/jrs.4037

[22] V. Hayez, V. Costa, J. Guillaume, H. Terryn, A. Hubin, Micro raman spectroscopy used for the study of corrosion products on copper alloys: study of the chemical composition of artificial patinas used for restoration purposes, Analyst, vol. 130 (2005) 4, pp. 550-556.
DOI: 10.1039/B419080G

[23] A. Salvini, D. Alloni, S. Altieri, N. Protti, M. Clemenza, Design, implementation and future utilization of the pgnaa facility at the university of Pavia–LENA laboratory, in Research Reactors: Addressing Challenges and Opportunities to Ensure Effectiveness and Sustainability. Summary of an International Conference. Supplementary Files, 2020.